2D and 3D Characterization of Damage Mechanisms in A319 Alloy

Alexis dos Santos, Jérôme Hosdez, Nathalie Limodin, A. El Bartali, A. Tandjaoui, Jean-Francois Witz, Christophe Niclaeys, Philippe Quaegebeur, Denis Najjar

2D and 3D characterization of damage mechanisms in A319 alloy

A. Dos Santos, J. Hosdez, N. Limodin, A. El Bartali, A. Tandjaoui, J.-F. Witz, C. Niclaeys, P. Quaegebeur, D. Najjar.

Univ. Lille, CNRS, Centrale Lille, UMR 9013 - LaMcube - Laboratoire de Mécanique, Multiphysique, Multiéchelle, F-59000 Lille, France

Corresponding author: Alexis Dos Santos, dossantos.alexis73@gmail.com

ABSTRACT

Background: Al-7Si-3Cu (A319) is used for automotive engine cylinder heads and the risk of cracking in the inter valve bridge of the cylinder head is high [1]. Due to the very slow cooling rate with Lost Foam Casting (LFC) foundry process, the alloy microstructure is coarse with shrinkage defects [2 - 7]. Previous studies show the key role of microshrinkage cavities in the initiation and the propagation of cracks: pores induce stress concentration in the close microstructure [8 - 20]. Objective: the aim of this work is to determine alloy damage at the microstructure scale in a model material with a simplified defect during a cyclic mechanical test. Methods: High Isostatic Pressing treatment and specific drilled hole were made on the sample test to control the crack initiation. A new speckle pattern was used for digital image correlation. The mechanical test was interrupted to couple 2D observations on the two sample surfaces with optical cameras and 3D observations with X-ray microtomography. Results: the resulting von Mises strain fields acquired *in situ* at the surface or *ex situ* in bulk show similarities and allow to study the strain evolution during a cyclic test. The study reveals crack initiation around the artificial hole in the gauge length of the specimen while propagation is mainly driven by the surrounding microstructure. Measured strain also allowed to identify the areas of damage and even to anticipate the cracking path. Conclusions: due to the microstructural complexity of a cast aluminum-silicon-copper alloy, the proposed approach based on a simplified defect material and two simultaneous observation methods with digital and volume image correlation is a strong advantage for quantitatively characterizing damage mechanisms at the microstructure scale.

KEYWORDS

Al-Si alloys; Mechanical cyclic test; Damage mechanisms; Digital image correlation; Digital volume correlation

EXPERIMENTAL PROCEDURE

To analyse microcrack initiation and propagation at a high spatial resolution in a limited observation area, all the pores in a sample cut from a cylinder head inter-valve bridge were closed with Hot Isostatic Pressing (HIP). The absence of porosity was controlled by X-ray microtomography at a fine resolution (voxel = 2.2 µm).Flat specimen has a representative microstructure of the Al-7Si-3Cu cylinder head alloy from LFC with a coarse dendritic structure (Secondary Dendrite Arm Spacing, SDAS = 75 µm). This hypoeutectic microstructure is composed of aluminum-rich alpha dendrites, eutectic silicon, copper (Al_2Cu) and iron-rich (α-AlFeMnSi and β-AlFeSi) constituents [21]. The gauge length has a square cross section of 2.5 x 2.5 mm² after mirror polishing. A circular through hole is drilled in the gauge length with a thin and hard drill bit made of tungsten carbide. The drilling machine has a high speed and slow feed with regular swarf removal in order to avoid material build-up on the hole surface. The surface finish quality was controlled with microtomography (2.2 µm voxel) before the test beginning to ensure that there are no cracks related to the drilling procedure. The hole is tilted by 6° thanks to an inclined holder made with 3D printing, hence it is centred on one surface of the specimen while it is off-center on the opposite surface (Fig. 2 for the hole geometry). Various holder tests were carried out but over 6° the drill bit broke. The goal is to increase the stress on the off-center surface and obtain microcrack initiation in the narrowest zone between the sample free surface and the hole. The last step is to make a speckle pattern on both drilled surfaces of the gauge length. The final aim is to perform Digital Image Correlation (DIC) at a small scale, *i.e.* at eutectic Si or intermetallics size. Contrary to the traditional pattern with airbrush [22] the paint is replaced by powder to obtain the speckle; the new protocol is:

- Spray black paint for the background.

- Spray speckle solution: 50 mg of a mixture of calcium carbonate and clay with 20 ml of ethanol.
- Drying time of 5 minutes.

The white speckle with the chalk mixture is finer than the paint speckle allowing to increase the pattern density hence contributing to a better measurement resolution for DIC. Indeed, the grey level variation inside the white spots is greater in chalk than in paint [23]. The size measurement of the white spots also reveals finer particles with the use of chalk (21µm on average) than with paint (33µm on average). For the displacement field measurement by Digital Volume Correlation (DVC), no sample preparation is required because the intermetallics, visible in the microtomography images, provide a natural speckle pattern.

The specimen is placed in the clamping jaws of a miniature tensile test rig Kammrath & Weiss (Fig. 1). In order to follow the two drilled surfaces during the test, two Ximea XiC cameras (12.4 Mpixels) with two Techspec Compact Tl telecentric lenses (magnification of x3) and two LED lights are used. A Python program controls the loading in displacement and the unloading to zero-load with a speed of 5 µm/s. The maximum displacement level increases in each cycle (see the top graph in Fig. 3). The test includes 31 cycles, *i.e.* 31 loadings and 31 unloadings, the last one corresponding to the sample final failure. The cameras take pictures on each load extremum during the cyclic test. The test is also interrupted at some unloading (eleven times in total) in order to scan the specimen in the microtomograph. This allows to complete the microstructure monitoring around the hole with 3D images acquired during elastic and plastic strain regimes. This strategy of combining surface and volume observation has already been used to determine the damage of specimens in a cyclic test and it proved to be complementary [24].

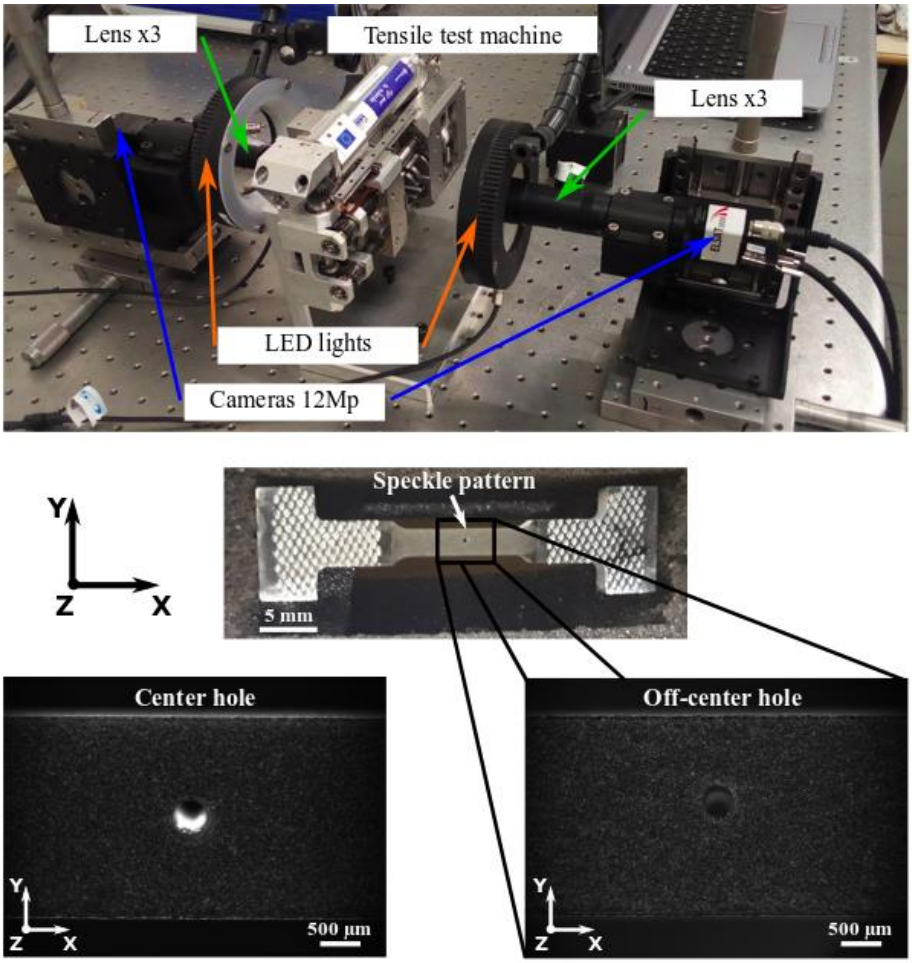

Figure 1: Experimental test device and test specimen with speckle pattern on the two drilled surfaces

Table 1 compares the characteristics of the two methods used to follow damage in the specimen microstructure: *in situ* optical monitoring and *ex situ* X-ray microtomography.

Observation	Optical cameras (2D)		Microtomography (3D)
Size	1.15 µm/pixel		2.22 µm/voxel
Region Of Interest (ROI)	4112 x 3008 pixels		1200 x 1200 x 1216 voxels
Recording time	< 1 second		30 minutes
Resolution measurement	DIC: 10 x 10 pixels		DVC: 16 x 16 x 16 voxels
Images acquisition	Before the test beginning and at each load and unload extremum		Before the test beginning and at the end of cycles 3, 7, 12, 15, 19, 21, 23, 26, 28, 30, 31
Displacement uncertainty	Center U: 0.17 pix. V: 0.24 pix.	Off-center U: 0.12 pix. V: 0.18 pix.	U: 0.06 vox. V: 0.04 vox. Z: 0.05 vox.
Strain uncertainty (X, Y, Z axis from Fig.1)	Center Exx = 0.002 % Eyy = 0.20 %	Off-center Exx = 0.064 % Eyy = 0.031%	Exx = 0.029 % Eyy = 0.024 % Ezz = 0.015 %

Table 1: Digital image and volume correlation settings

Optical surface monitoring has a higher measurement resolution than X-ray microtomography due to a better spatial resolution of the optical images and an improved speckle pattern. It also allows following a larger area of the gauge length (4.7 mm x 3.5 mm) with a quick recording time in contrast to the microtomography scan (2.7 mm x 2.7 mm x 2.7 mm). Another advantage is the possibility to link the eutectic silicon with damage mechanisms (observed *post mortem* with SEM) and strain localization measured *in situ* with DIC. Because of their close atomic number, silicon has an X-ray absorption coefficient close to aluminum. This leads to low contrast on the X-ray microtomography images between eutectic Si and Al from the alpha phase of primary aluminum (dendrites) and eutectic aluminum. Moreover, the low contrast difference between the copper and iron intermetallics also causes difficulty in post-processing constituents' identification. The optical microscope mapping of the two drilled surfaces before spraying the speckle pattern allows to overlay the finely resolved optical microstructure with the displacement field from DIC and to identify the behaviour of all constituents.

DIC and DVC measurements were performed with YaDICs (Yet another Digital Image Correlation software), a homemade programming platform [12] [13] [25]. Digital image and volume correlation consist in finding the transformation between an initial and a deformed image for measuring displacement fields. Here, the initial image is the picture acquired at the test beginning with a 0N load. The moving image corresponds to the different steps of the mechanical test either at maximum or minimum load (Fig. 3); the computed strains shown hereafter are then cumulative strains. In this study, the metric is based on the Sum of Squared Differences (SSD) completed by an optimisation strategy via the gradient algorithm. A bi-cubic interpolator applies this transformation to the deformed image at each iteration by evaluating the grey levels of this image. The resolution is based on a multi-scale strategy in pyramid form and global displacements are determined using finite element functions [26]. Fields regularization is applied with a median filter of 7 pix/vox (more details in [27]). A rigid body movement was applied on the specimen before the test in order to determine the uncertainty of the displacement fields (Tab.1) [12] [28] and to demonstrate the feasibility of DIC and DVC with the A319 alloy. The measurement resolution choice in DIC (10x10) and DVC (16x16x16) was determined by the convergence of the digital correlation calculation: a smaller element size causes a non-physical field discontinuity in the results. Results of DIC measurements were validated on a comparative test with a specimen equipped by a strain gauge [23].

RESULTS AND DISCUSSION

The designed hole allowed a preferential initiation of microcracks at the hole surface but the inclination was not sufficient to generate a single crack on the specimen surface (Fig. 2). Analysis of X-ray microtomography slices through the whole thickness reveals microcracks on the off-center surface but also in volume. Thus, in the plastic regime, multiple microcracks initiation occurs. Furthermore, fracture surface investigation with Scanning Electron Microscope (SEM) shows that the additive elements such as silicon, copper and iron impurity, which reflect the presence of eutectic Si, copper and iron based intermetallics respectively, are characterised by brittle fracture. Only the primary α-phase of aluminum shows ductility with some dimples but at

a local scale. The brittleness of the Si and intermetallic compounds did not allow the asymmetrical defect to enforce the fracture initiation.

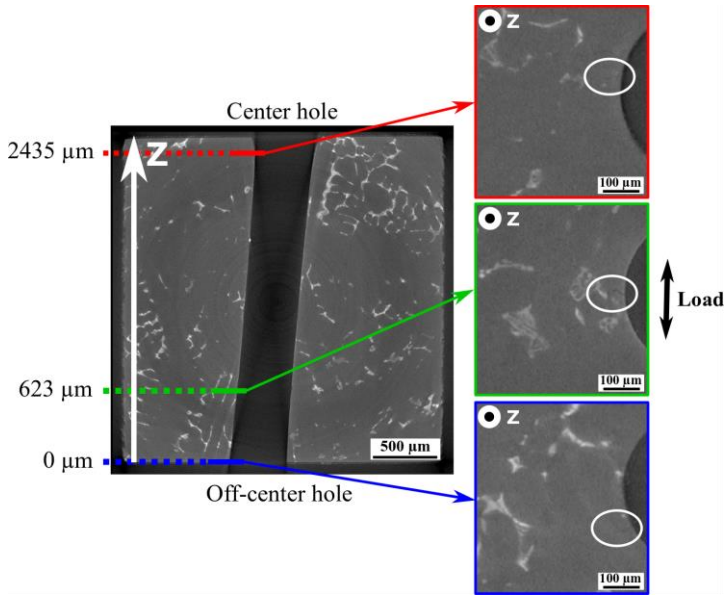

Figure 2: X-ray microtomography slice at the hole cross section (on the left) and slices perpendicular to the z axis at different depths (on the right) showing multiple microcracks initiation along the hole after the 28th cycle

This overview of the cyclic test shows the necessity of 3D images to study the damage mechanisms. The first microcrack observed is located in the thickness of the specimen at a depth of 623 µm (Fig. 3). The limited cycles number between crack initiation (27th or 28th cycle) and fracture confirms the material brittleness. The microcrack starts at the edge of the hole in the Al-Si matrix. The path of the final crack in cycle 31 shows that propagation occurs preferentially in the iron-rich intermetallics. The superposition of the strain fields calculated by DVC with the corresponding tomography slices allows establishing several observations for the three last microtomography scans at unloaded state before failure. The residual von Mises strain values increase progressively with the applied load: from 1% at cycle 26, they reach locally nearly 4% before cycle 31. Locally high levels of strain can be reached early in the test. High strains correspond to the location of the microcrack whose propagation seems to be correlated to the areas of the highest local strain recorded in the previous cycle.

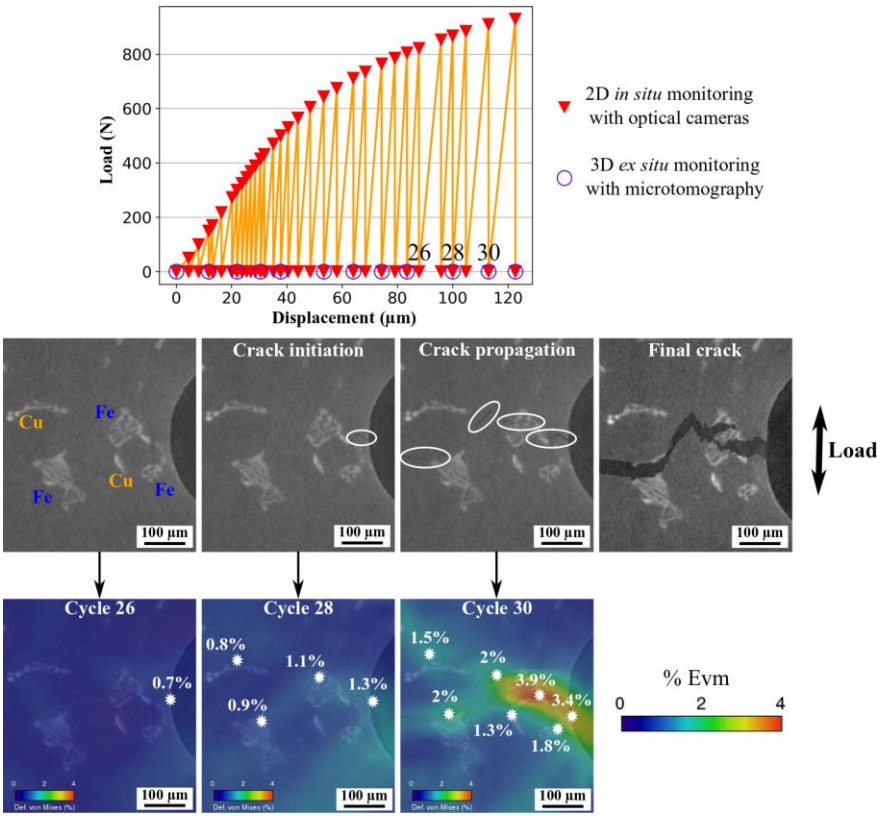

Figure 3: X-ray microtomography slices (depth of 623 µm) and von Mises strain calculated from DVC displacement fields measurement at different steps of the test

To compare DVC and DIC at the surface of the sample, the optical image was registered (rigid body motion and scaling) with the corresponding microtomography slice. As the acquisition method is not identical, the two images do not have the same dimensions and orientation. Thus, a Python program is used to detect the edges of the specimen and the hole. It is then possible to correct the angle of rotation, to modify the scale and to apply a rigid body movement to the optical image to superimpose perfectly the surface of the specimen on the 2D image with the same surface on the tomographic slice. Strains were calculated by applying the derivative of the displacement fields in a Python program. The resulting registered DVC and DIC von Mises strain fields at the unloaded state on the surface with the off-center hole (Fig. 4) confirm the stress concentration effect of the hole with residual plasticity that increases throughout the test. Both methods give similar fields with identical deformation levels. However, the higher resolution reached with the optical camera means that the local deformations are less smooth than with DVC. Hence, the strain heterogeneity is better studied in 2D images. Image correlation is a sensitive measure and noise may appear on the results. The 2D strain fields on some cycles may show measurement errors locally. Consequently, only DIC and DVC results in a restricted area showing similar tendency were considered to ensure the analysis is related to physical phenomenon and not to numerical noise.

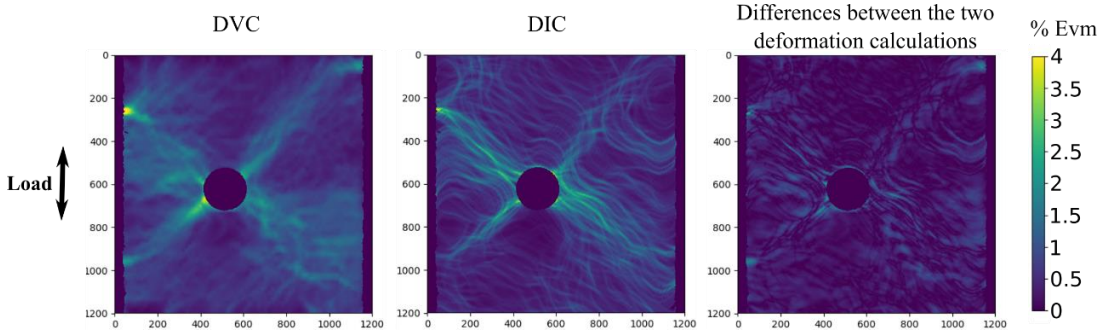

Figure 4: von Mises Strain fields from DVC and DIC at the off-center hole surface after the 30th cycle before the final failure of the sample (size in pixels × pixels)

To take advantages of the DIC, another area with a microcrack was selected to observe the damage of an intermetallic close to the hole edge at the specimen surface. This zone contains eutectic silicon and intermetallics rich in copper and iron. *Post mortem* images from SEM (Fig. 5 (a)) show a microcrack between two intermetallics near the final crack initiation site at the hole periphery. The 3D monitoring indicates that this crack appears at the end of the test during the last loading before failure.

The von Mises strain fields calculated by DIC at different loads during the test are projected on the X-ray microtomography slice to follow the strains evolution at intermetallics (Fig. 5 (a)). Before the final crack on the cycle 30 (load of 986N), the most deformed area is located on a copper intermetallic. A high-level strain band (Fig. 5 (b)) is however visible between iron and copper intermetallics, *i.e.* at the position of the future microcrack. A maximum strain higher than 4%, an increase of nearly 80% compared to the previous measurement, is then measured at the surface during the failure of the specimen (cycle 31); this large strain corresponds to crack opening (Fig. 5 (c)).

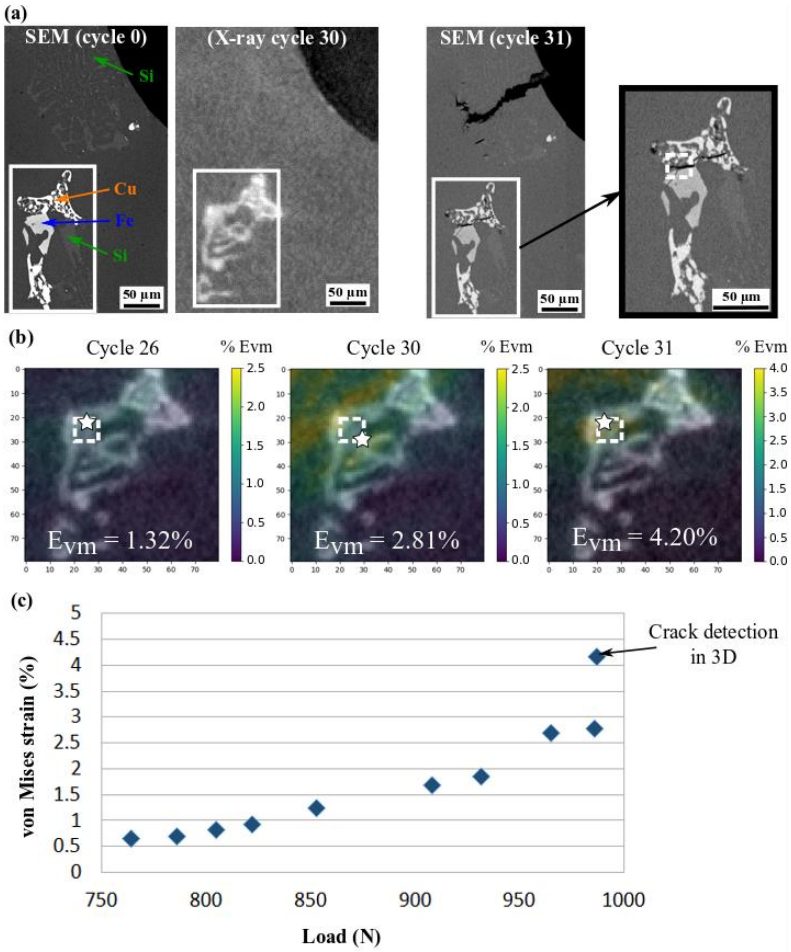

Figure 5: Focus on some intermetallics before the start of the cyclic test (cycle 0), before the final crack (cycle 30) and in post-mortem analysis (cycle 31) (a). Von Mises strains fields measured with DIC at the last cycles of the test and position of the maximum value (indicated with star symbols) (b). Evolution of the maximum von Mises strain during the cyclic test (c)

CONCLUSION

Al-Si-Cu alloy has a complex microstructure but the importance of rigid inclusions in the cracking phenomenon has been highlighted. Crack initiation occurs on the "artificial defect" and propagation depends on the surrounding microstructure. As a result, drilling a non-symmetrical hole in the structure did not create a single crack initiation zone. This study used two complementary measurement methods to calculate the deformation fields: DVC and DIC. 3D observations are required to have a monitoring along the hole due to the presence of multi-cracking during the mechanical test while 2D observations allow access to more resolved and continuous information in time thanks to *in situ* recording. Strain fields revealed the plasticity evolution in the microstructure during the

mechanical test. It also allowed to identify the areas of damage and even to predict the cracking path at the scale of the microstructure. As indicated in the literature, the brittle microstructure constituents appear to have a strong influence on the propagation path, in particular eutectic silicon which has the lowest deformations before failure.

ACKNOWLEDGEMENTS

The authors wish to thank Centrale Lille, Hauts de France region and ELSAT2020 for funding the PhD thesis of Alexis Dos Santos and some of the equipment. The authors would like to thank also ISIS4D (https://isis4d.univ-lille.fr/) X-Ray CT platform (Lille, France) for making the *ex situ* test possible.

Ethics declarations

Conflict of interest: the authors have no conflicts of interest to declare.

REFERENCES

[1] Szmytka F, Oudin A (2013) A reliability analysis method in thermomechanical fatigue design. International Journal of Fatigue 53:82-91. https://doi.org/10.1016/j.ijfatigue.2012.01.025

[2] Chen R, Shi YF, Xu QY, Liu BC (2014) Effect of cooling rate on solidification parameters and microstructure of Al-7Si-0.3Mg-0.15Fe alloy. Transactions of Nonferrous Metals Society of China 24:1645–1652

[3] Dobrzański LA, Maniara R, Sokołowski J, Kasprzak W (2007) Effect of cooling rate on the solidification behavior of AC AlSi7Cu2 alloy. Journal of Materials Processing Technology 191:317-320. https://doi.org/10.1016/j.jmatprotec.2007.03.099

[4] Kang SB, Zhang J, Wang S, Cho J, Stetsenko VU (2010) Effect of Cooling Rate on Microstructure and Mechanical Properties in Al-Si Alloys. Proceedings of the 12th International Conference on Aluminium Alloys 675-680

[5] Akhil K, Arul S, Sellamuthu R (2014) The Effect of Section Size on Cooling Rate, Microstructure and Mechanical Properties of A356 Aluminum Alloy in Casting. Procedia Materials Science 5:362-368. https://doi.org/10.1016/j.mspro.2014.07.278

[6] Ceschini L, Morri A, Toschi S, Seifeddine S, Messieri S (2017) The influence of cooling rate on microstructure, tensile and fatigue behavior of heat-treated Al-Si-Cu-Mg alloys. Materials Science Forum 884:81-92. https://doi.org/10.4028/www.scientific.net/MSF.884.81

[7] Vandersluis E, Ravindran C (2018) Relationships between solidification parameters in A319 aluminum alloy. Journal of Materials Engineering and Performance 27:1109-1121. https://doi.org/10.1007/s11665-018-3184-2

[8] Dezecot S, Buffiere JY, Koster A, Maurel V, Szmytka F, Charkaluk E, Dahdah N, El Bartali A, Limodin N, Witz JF (2016) In situ 3D characterization of high temperature fatigue damage mechanisms in a cast aluminum alloy using synchrotron X-ray tomography. Scripta Materialia 113:254-258. https://doi.org/10.1016/j.scriptamat.2015.11.017

[9] Zhang C, Poirier B (2001) Effect of solidification cooling rate on the fatigue life of A356 T6 cast aluminum alloy. Fatigue and fracture of engineering materials and structures 23:417-423. https://doi.org/10.1046/j.1460-2695.2000.00299.x

[10] Wang L, Limodin N, El Bartali A, Witz JF, Seghir R, Buffiere JY, Charkaluk E (2016) Influence of pores on crack initiation in monotonic tensile and cyclic loadings in lost foam casting A319 alloy by using 3D in-situ analysis. Materials Science and Engineering: A 673:362-372. https://doi.org/10.1016/j.msea.2016.07.036

[11] Liu F, Zhao HD, Yang R, Sun F (2019) Crack propagation behavior of die-cast AlSiMgMn alloys with in-situ SEM observation and finite element simulation. Materials Today Communications 19:114-123. https://doi.org/10.1016/j.mtcomm.2019.01.009

[12] Dahdah N, Limodin N, El Bartali A, Witz JF, Seghir R, Buffiere JY, Charkaluk E (2016) Damage Investigation in A319 Aluminium Alloy by X-ray Tomography and Digital Volume Correlation during In Situ High-Temperature Fatigue Tests. Strain 52:324-335. https://doi.org/10.1111/str.12193

[13] Li Z, Limodin N, Tandjaoui A, Quaegebeur P, Witz JF, Balloy D (2020) In-situ 3D characterization of tensile damage mechanisms in A319 aluminum alloy using X-ray tomography and digital volume correlation. Materials Science and Engineering: A 794:139920. https://doi.org/10.1016/j.msea.2020.139920

[14] Li Z, Limodin N, Tandjaoui A, Quaegebeur P, Witz JF, Balloy D (2016) Damage investigation in A319 aluminum alloy by digital image correlation during in-situ tensile tests. Procedia Structural Integrity 2:3415-3422. https://doi.org/10.1016/j.prostr.2016.06.426

[15] Le VD, Saintier N, Morel F, Bellett D, Osmond P (2018) Investigation of the effect of porosity on the high cycle fatigue behaviour of cast Al-Si alloy by X-ray micro-tomography. International Journal of Fatigue 106:24-37. https://doi.org/10.1016/j.ijfatigue.2017.09.012

[16] Arami H, Khalifehzadeh R, Akbari M, Khomamizadeh F (2008) Microporosity control and thermal-fatigue resistance of A319 aluminum foundry alloy. Materials Science and Engineering: A 472:107-114. https://doi.org/10.1016/j.msea.2007.03.031

[17] Le VD, Morel F, Bellett D, Saintier N, Osmond P (2016) Multiaxial high cycle fatigue damage mechanisms associated with the different microstructural heterogeneities of cast aluminium alloys. Materials Science and Engineering: A 649:426-440. https://doi.org/10.1016/j.msea.2015.10.026

[18] Nicoletto G, Konečná R, Fintova S (2012) Characterization of microshrinkage casting defects of Al–Si alloys by X-ray computed tomography and metallography. International Journal of Fatigue 41:39-46. https://doi.org/10.1016/j.ijfatigue.2012.01.006

[19] Wicke M, Luetje M, Bacaicoa I, Brueckner-Foit A (2016) Characterization of Casting Pores in Fe-rich Al-Si-Cu Alloys by Microtomography and Finite Element Analysis. Procedia Structural Integrity 2:2643-2649. https://doi.org/10.1016/j.prostr.2016.06.330

[20] Serrano-Munoz I, Buffiere JY, Verdu C (2018) Casting defects in structural components: Are they all dangerous? A 3D study. International Journal of Fatigue 117:471-484. https://doi.org/10.1016/j.ijfatigue.2018.08.019

[21] Tabibian S, Charkaluk E, Constantinescu A, Szmytka F, Oudin A (2013) TMF–LCF life assessment of a Lost Foam Casting A319 aluminum alloy. International Journal of Fatigue 53:75-81. https://doi.org/10.1016/j.ijfatigue.2012.01.012

[22] Li Z, Limodin N, Tandjaoui A, Quaegebeur P, Witz JF, Balloy D (2017) Influence of Fe content on the damage mechanism in A319 aluminum alloy: Tensile tests and digital image correlation. Engineering Fracture Mechanics 183:94-108. https://doi.org/10.1016/j.engfracmech.2017.05.006

[23] Dos Santos A (2021) Étude des mécanismes d'endommagement de la microstructure d'un alliage d'aluminium-silicium pour application automobile à partir d'éprouvette modèle à défaut contrôlé. PhD thesis.

[24] Vrgoč A, Tomičević Z, Smaniotto B, Hild F (2021) Application of different imaging techniques for the characterization of damage in fiber reinforced polymer. Composites Part A: Applied Science and Manufacturing 106576-150. https://doi.org/10.1016/j.compositesa.2021.106576

[25] Hosdez J, Langlois M, Witz JF, Limodin N, Najjar D, Charkaluk E, Osmond P, Forre A, Szmytka F (2019) Plastic zone evolution during fatigue crack growth: Digital image correlation coupled with finite elements method. International Journal of Solids and Structures 171:92-102. https://doi.org/10.1016/j.ijsolstr.2019.04.032

[26] Besnard G, Hild F, Roux S (2006) “Finite-Element” Displacement Fields Analysis from Digital Images: Application to Portevin – Le Châtelier Bands. Experimental Mechanics 46:789-803. https://doi.org/10.1007/s11340-006-9824-8

[27] Seghir R, Witz JF, Coudert S (2014) YaDICs. https://en.wikipedia.org/wiki/YaDICs

[28] Limodin N, Réthoré J, Adrien J, Buffiere JY, Hild F, Roux S (2011) Analysis and artifact correction for volume correlation measurements using tomographic images from a laboratory X-ray source. Experimental Mechanics 51:959-970. https://doi.org/10.1007/s11340-010-9397-4